In Memoriam
of E.P. Abranin and L.L. Baselyan

DOI: https://doi.org/10.15407/rpra28.02.095
UDC 523.985.7-77+523.947+520.27

A.A. Stanislavsky [1], A.A. Koval [2], I.N. Bubnov [1], and A.I. Brazhenko [3]

[1] Institute of Radio Astronomy NAS of Ukraine
4, Mystetstv St., Kharkiv, 61002, Ukraine
E-mail: a.a.stanislavsky@rian.kharkov.ua
[2] Astronomical Institute of the Czech Academy of Sciences
Fričova 298, 251 65 Ondřejov, Czech Republic
[3] Poltava Gravimetric Observatory, Subbotin Institute of Geophysics NAS of Ukraine
27/29, Myasoyedov St., Poltava, 36029, Ukraine

PROGRESS IN THE STUDY OF DECAMETER-WAVELENGTH SOLAR RADIO EMISSION WITH UKRAINIAN RADIO TELESCOPES. Part 1*

Subject and Purpose. *Results are presented of the solar corona investigations performed with the world famous Ukrainian radio telescopes. The work has been aimed at offering a consistent review of recent achievements in observations of a variety of low-frequency radio emissions from the Sun.*

Methods and Methodology. *The studies of the quiet (thermal) and sporadic (burst-like) radio emissions from the Sun have been carried out with the decameter-wavelength radio telescopes UTR-2, GURT and URAN-2. Specific features of the low-frequency solar radio emissions from a variety of sources are presented, with characterization of the optimized techniques that were applied in each case for evaluating physical parameters of the corona in the areas of decameter-wavelength radio wave generation.*

Results. *The analysis of temporal, frequency and spatial characteristics of solar radio emissions has allowed suggesting a number of models for the coronal electron density distribution, and evaluating magnetic field strengths in the corona. Also, our experimental results have proven to be consistent with the observational data obtained in different frequency ranges and with the use of both ground based and space-borne instruments.*

Conclusions*. The radio observations performed with Ukrainian radio telescopes have permitted studying, with high temporal, frequency and spatial resolutions, solar radio frequency emissions from various localized sources. Along with the large effective area and high sensitivity of the antennas, this permits application of a wide range of methods and tools aimed at detecting and analyzing solar bursts, of both strong and weak intensity, against the background of terrestrial interference of natural or artificial origin.*

Keywords: *the Sun, decameter-wavelength radio emission, radio bursts, solar corona, UTR-2, URAN-2, GURT.*

* Invited paper.

Citation: Stanislavsky, A.A., Koval, A.A., Bubnov, I.N., and Brazhenko, A.I., 2023. Progress in the study of decameter-wavelength solar radio emission with Ukrainian radio telescopes. Part 1. (Invited paper). *Radio Physics and Radio Astronomy*, **28**(2), pp. 95—116. https://doi.org/10.15407/rpra28.02.095

Цитування: Станиславський О.О., Коваль А.О., Бубнов І.М., Браженко А.І. Досягнення у вивченні декаметрового радіовипромінювання Сонця за допомогою українських радіотелескопів. Частина 1. (Стаття на замовлення). *Радіофізика і радіоастрономія*. 2023. Т. 28. № 2. С. 95—116. https://doi.org/10.15407/rpra28.02.095

Introduction

The Sun is the most powerful source of emissions in the radio sky. The research concerning this radiation has been going on for over 70 years since the emergence of radio astronomy as a science. The Sun, as the closest star to us, is being explored in various ways and with many instruments. Without doubt, the contribution of space missions, such as STEREO, Wind/WAVES, Parker Solar Probe and other to this study is enormous. Nevertheless, the role of ground-based radio astronomy in the exploration of low-frequency solar radiation is still extremely important. There are several reasons for this. While the radio instruments of space missions permit observing radio emissions at frequencies below the ionospheric cutoff, their records may often have a forbiddingly low time-frequency resolution. Unfortunately, the space-based antennas are of the simplest, whip forms. Their sensitivity is not as high as shown by array antennas. This explains why there is great interest toward projects of constructing very low-frequency antenna arrays on the far-side of the Moon. In this respect, the Ukrainian ground based radio telescopes UTR-2, URAN and GURT stand out. Operating at decameter and meter wavelengths, they are the only instruments in the world that can receive, with high time-frequency resolution and sensitivity, radio emissions at frequencies up to 8—10 MHz. This achievement owes not to the excellent broadband antennas (best in the frequency range) alone, but also to the superior digital receivers demonstrating a high dynamic range. Many of the solar radio bursts are characterized by a fine structure which is impossible to identify and investigate without such instruments. Despite the fact that the possibility of carrying out observations at frequencies below 20 MHz was announced by operators of such radio telescopes as LOFAR (Holland), LWA (USA), MWA (Australia), NenuFAR (France), their capabilities are still inferior to Ukrainian radio telescopes.

The aim of this paper is to present an integrative overview of the principal results lately obtained by the authors with the aid of the Ukrainian radio telescopes, cherishing the hope it would be useful for a wide range of readers. The review consists of two parts. Part 1 is devoted mainly to low-frequency observations of the quiet Sun and various types of solar bursts.

1. Heliograph

Historically, the first setup of a radio heliograph using the UTR-2 was implemented in the 1970s (see paper [1] and references therein). The critically important role in the initiative was played by E.P. Abranin. It was he who made the development and implementation of an extra phase shifting module for the device [2]. The spatially resolved observations of type IIIb-III and type IIId solar bursts were performed with a telautograph in the capacity of recording equipment. Unfortunately, the heliographic observations were realized only at a few individual frequencies, while the UTR-2 antenna is a broadband system. The approach was of certain interest as the first-of-its-kind endeavor, but its capabilities were rather limited by the then state of the art in the low-frequency radio astronomy. The design required cardinal improvements. Therefore, the UTR-2-based heliographic research was stopped in mid-1990s. A new breath for the project on the development of a UTR-2-based heliograph opened in 2009 [3, 4]. The concept was to improve the instrument via employment of a hybrid scheme, i.e. by taking the best features of the analog part (specifically, the signal phasing system of the UTR-2) and profiting by the latest achievements of computer electronics (like effective integrated circuits) [5]. The operation of the heliograph is based on a simple principle, namely sequential scanning of the sky area under investigation with the pencil-shaped beam of the UTR-2 [6]. The method has advantages and disadvantages alike. On the one hand, the implementation of this device is relatively simple and not very expensive. However, the sequential regime does not permit using the UTR-2 for standard spectrogram observations, because the heliograph is embedded in the UTR-2 and, in the course of making heliograms, the pencil-shaped beam of the radio telescope quickly changes its position on the sky around the Sun. At the same time, the amount of data turns out to be huge, and so far it has not been possible to obtain any heliograms in real time. The latter would require additional modernization of numerical receivers used with the UTR-2. Nevertheless, this did not interfere with new heliographic radio observations of either the quiet Sun or solar bursts [7—9], although they remain rather time-consuming (with regard to the final result). In the sections to follow they will be considered in detail.

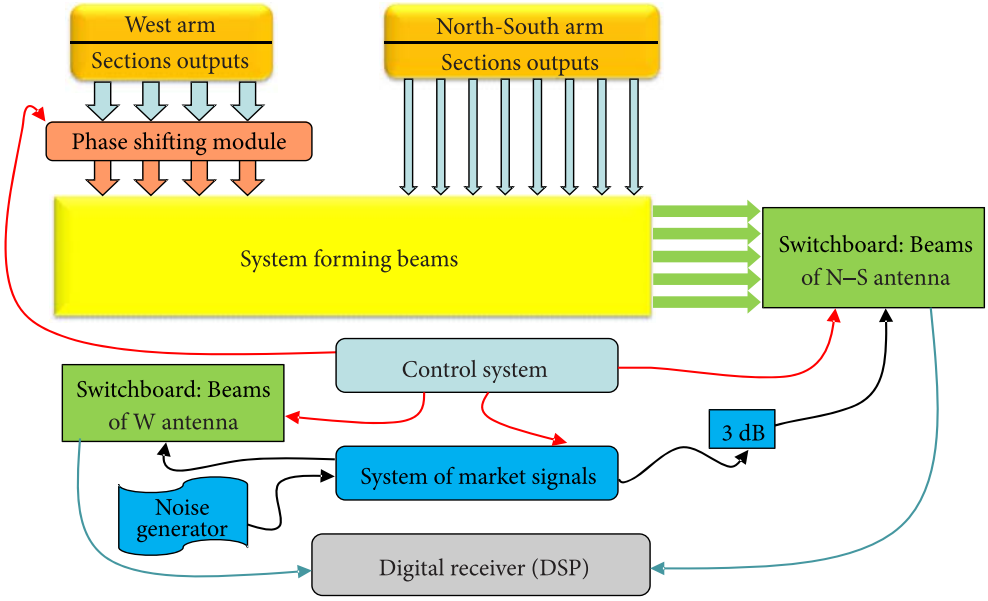

Fig. 1. Block diagram of the UTR-2 heliograph

The broadband T-shaped radio telescope (known as the UTR-2) consists of two antenna arrays, specifically the "North-South" and the "West", involving two thousand and forty wide-band dipoles. The Ukrainian telescope is capable of operating either in the multi-beam or single-beam regime. Through the use of the five independent pencil-shaped beams spaced in declination, the solar heliograph of the UTR-2 allows performing radio imaging of the solar corona at decameter wavelengths. To shape the pencil beams, the signal from the "West" antenna output is to be multiplied by signals from the five beam outputs of the "North-South" antenna with the help of a two-channel receiver-and-recorder device (abbreviated as DSP for "Digital Spectro-Polarimeter"). This allows using the antenna array in a 2D heliograph with either serial or parallel-serial scanning. In the serial regime the output signals from the five beams are recorded one after another in one and the same DSP, and the five beams of the antenna pattern are moved along the sky. The parallel-serial scanner system employs five parallel receiver channels for simultaneously recording the signals from the five beams. Note that the fully parallel mode (capable of instantly recording the full heliograph frame) is possible too, but it takes too much DSP resources. Although the UTR-2 radio telescope was created as a multi-task instrument, its phasing system which employs electromagnetic relays, does not allow for long-term observations in the fast beam scanning regime suitable for heliographic purposes. This disadvantage has been done with by introduction of an additional phasing system to make the fast beam scanning. Its phase shifting module is located between the sectional outputs and their respective inputs in the final phasing stage of the array "West". Consequently, the sectional pattern represents an envelope of all (five) patterns belonging to the scanning beams. The main task of this module is to swiftly change the antenna pattern's orientation selecting one from among eight discrete positions. The extra phase shifting module combines four identical parts. Each of these involves a three-digit discrete-binary time-delay cable line (Fig. 1). The line segments of the coaxial cables are switched by pin-diodes. The cable lines differ only in the values of time delays. A feature of the serial and parallel-serial scanning processes is generation of separating markers. The marker signals are intended for indicating each of the five-beam signals as well as for marking the beginning (or end) for each frame of the heliogram (consisting of 5×8 pixels). The signal magnitudes of the markers for frame beginning (ending) are higher than of the markers between five-beam signals due to the presence of a 3 dB attenuator in the circuit. All this allows us to easily recover heliogram images from their DSP records. In fact, the core of the control system for the UTR-2-based heliograph is its

"finite state machine" realized with chips. It forms driver signals (by means of a DDS — Direct Digital Synthesizer) for the extra phase shifting module and interacts with a microcontroller.

2. Quiet Sun

2.1. One-dimensional heliographic investigations

The low-frequency solar radio emission is represented by two important components, namely the quiet and the sporadic one. They are characterized by differing generation mechanisms. The first of them is thermal in nature, and its intensity decreases toward lower frequencies. When solar activity is at its minimum, the nature of radio emission is close to thermal. These conditions are favorable for low-frequency observations of the quiet Sun. The correspondent emissions are of weak enough intensity, hence observable with antenna systems of sufficiently high effective areas. The UTR-2, URAN and GURT antennas are just suitable for the purpose.

In the study of quiet solar emission we used different methods. They included one-dimensional and two-dimensional heliographic observations as well as records of the solar eclipse. Their results are considered in more detail below. The one-dimensional heliographic investigations employ the simple technique of scanning the Sun with a fixed antenna beam [10, 11]. Note that a radio Sun observed during its minimum activity looks like an extended source (> 30 arc minutes) of rather homogeneous apparent structure and of size in excess of the solar radius. Under these conditions, it looks stretched equatorially because the solar atmosphere has a larger electron density at the equator than at the poles. This fact allows performing its diagnostics through investigations of the radio continuum. In the absence of solar flares, it is the non-coherent radiation from the thermal coronal plasma which is the source of the radio emission. Therefore, the radio brightness demonstrated by the Sun is globally determined by the thermal scattering due to electron-ion collisions in the corona. During the 2008—2009 observation campaign, the measurements with the URAN-2 radio telescope were simultaneously made at two frequencies, 20 and 25 MHz. Over the periods of those observations, active regions on the solar disk were absent. At decameter wavelengths, the variations observable in the total flux density of the solar radio emission are caused not only by activity variations, but also by the radio wave attenuation in the ionosphere and refraction by ionospheric irregularities. Average magnitudes of the decrease in flux density usually are to be taken into account during observations of a powerful point source whose position on the celestial sphere and time of observation is as close as possible to such of the measured object. The well-known radio source Taurus A (3C144) was selected as such a source. The values obtained for the radiation flux density of this source were about 2 870 Jy at 25 MHz and 3 430 Jy at 20 MHz. These values are in agreement with the data observed with the UTR-2. Upon removal of the radio-frequency noise, more than 2 500 samples of flux density of the continuum radio emission at 20 MHz, and almost 3 200 samples at 25 MHz were obtained. The averaged values equaled 710 and 860 Jy for these two frequencies, respectively, with an error no more than ±18%. Generally, the URAN-2 measurements are in good agreement with the data observed with the telescopes operating in other frequency ranges. If the data are plotted together within the band between 20 and 200 MHz, then the spectral index of the solar quiet radio emission is equal to -2.1 ± 0.1, which is very close to the spectral index for the long-wavelength blackbody radiation. The reason is that the angular size of the radio Sun grows with the wavelength, while its brightness temperature drops down.

The quiet-Sun radio emission was investigated with the UTR-2 antenna system on Sept. 4 to Sept. 6, 2010. To obtain scans of the continuum radiation, the five-beam mode of the UTR-2 array was used. The middle beam (beam three from left to right or vice versa) was directed toward the center of the solar disk in declination, and then turned away from it in hour angle. The duration of each scan was 30 min. Over that time, the solar disk crossed the main lobe of the telescope's pattern because of the Earth's rotation. Through the period of observations, more than twenty 30-minute scans were obtained. The measurements were made within the bandwidth of 16.5 to 33 MHz, with a time resolution about 100 ms. The flux density values of the radio emission received were determined using calibration by the known spectral power values of the noise-generator, as well as through calculation of the UTR-2 effective area in dependence of the Sun's position on the celestial

sphere. The obtained profiles are well approximated to a one-dimensional Gaussian function. It should be pointed out that the profiles included contributions from strong solar bursts as well. Fortunately, these were observed rarely enough and did not noticeably distort the shape of the recorded profiles. Accordingly, the spectral index within the bandwidth of 18 to 200 MHz could be estimated as -2.1 ± 0.1, which is in agreement with the index value determined from the URAN-2 measurements mentioned above. Here it is worthy of note that the UTR-2 observations have been performed through a continuous frequency band, specifically 16.5 to 33 MHz, unlike the URAN-2 observations made in a narrow band mode at two isolated frequencies. To make comparison with the URAN-2 observations, we also have taken the UTR-2 results measured at the same frequencies, i.e. 20 and 25 MHz. The flux density values measured with the UTR-2 turned out to be somewhat higher. The explanation is that in 2008–2009 the Sun was at a deep minimum of activity, whereas the year 2010 marked its increase at the initial phase of the 11-year cycle. The angular equatorial diameters of the Sun's radio image at 16.5—33 MHz, as measured with the UTR-2, changed, on average, from 90 to 65 arc minutes.

2.2. Solar eclipse

The solar eclipse of August 1, 2008 fell on a deep minimum of solar activity. No active areas were observed in the solar photosphere. Using the decametre-wavelength radio telescopes URAN-2 and URAN-3 [12], radio observations were performed of the partial solar eclipse. An important feature of the observations was that they were performed with two radio telescopes at a time. The URAN-2 and URAN-3 are similar in technical characteristics, however located at a distance of about 805 km. The visible radius of the solar disk during the eclipse was 15′45″, while the visible disk of the Moon was 16′14″. The solar corona was assumed to have the form of an ellipse with the major axis of 57′ in the equatorial plane and the minor axis of 41′ within the polar plane (as measured at 25 MHz). With such parameters of the corona, the maximum decrease in the intensity of coronal radiation (owing to the eclipse by the Moon) cannot exceed 45%. In the case of the URAN-2, the real relative area of the coronal patch covered by the Moon (during the August 1, 2008 eclipse) was in the range of 0.21–0.26. For the location of the URAN-3, the maximum magnitude of the visible solar disk was 25%, while at the culmination time the value reached 11.5%. According to the observations, the ratio of the flux density of the Moon-masked Sun to the unmasked flux density at $f = 20.75$ MHz was 0.89 ± 0.03, whereas at $f = 23.9$ MHz the value was 0.82 ± 0.02. Also, the flux density of the solar emission observable on August 1, 2008 was measured as 620 ± 100 Jy at 20.75 MHz and 715 ± 100 Jy at 23.9 MHz. The August 1, 2008 observations of the solar eclipse were also performed with the UTR-2 radio telescope, however, because of some technical problem they were not successful. Therefore, we can only mention them as an attempt.

2.3. Two-dimensional heliographic studies

Interesting results concerning the quiet Sun corona were obtained through the use of the two-dimensional heliograph described in the previous Section [1—4]. The angular sizes of the radio heliograms recorded at 25 MHz measure as 2.1° and 3.3° along declination and hour angle, respectively. The radio images of the solar corona were obtained during observations with the UTR-2 that lasted from August 28 till September 3, 2010. At the period, the solar activity was weak. The single bursts during the observation campaign did not prevent achieving the basic aim of these observations. The solar corona being observed with a decameter wavelength heliograph appears as an extended source of radio emission. Therefore, the source represented on the heliographic frames seems to be "distributed" over several elements (or pixels). Recall that one of the major tasks implied by application of a heliograph consists in observations of 2-D distributions of the undisturbed corona brightness. The slow Sun tracking rate was taken equal to 16 min. For this time, a point source (such as, for example, 3C144, 3C274 or 3C405) would traverse the heliogram frame from its one edge to the opposite side. The switching rate of the fast scanning phase shifter was taken such that each heliograph image could be formed for 2 min. This was enough for the case considered, where changes in the position of both point-like and extended source were produced mainly by the celestial sphere's diurnal motion. Such magnitudes of the image formation rate and source tracking time have

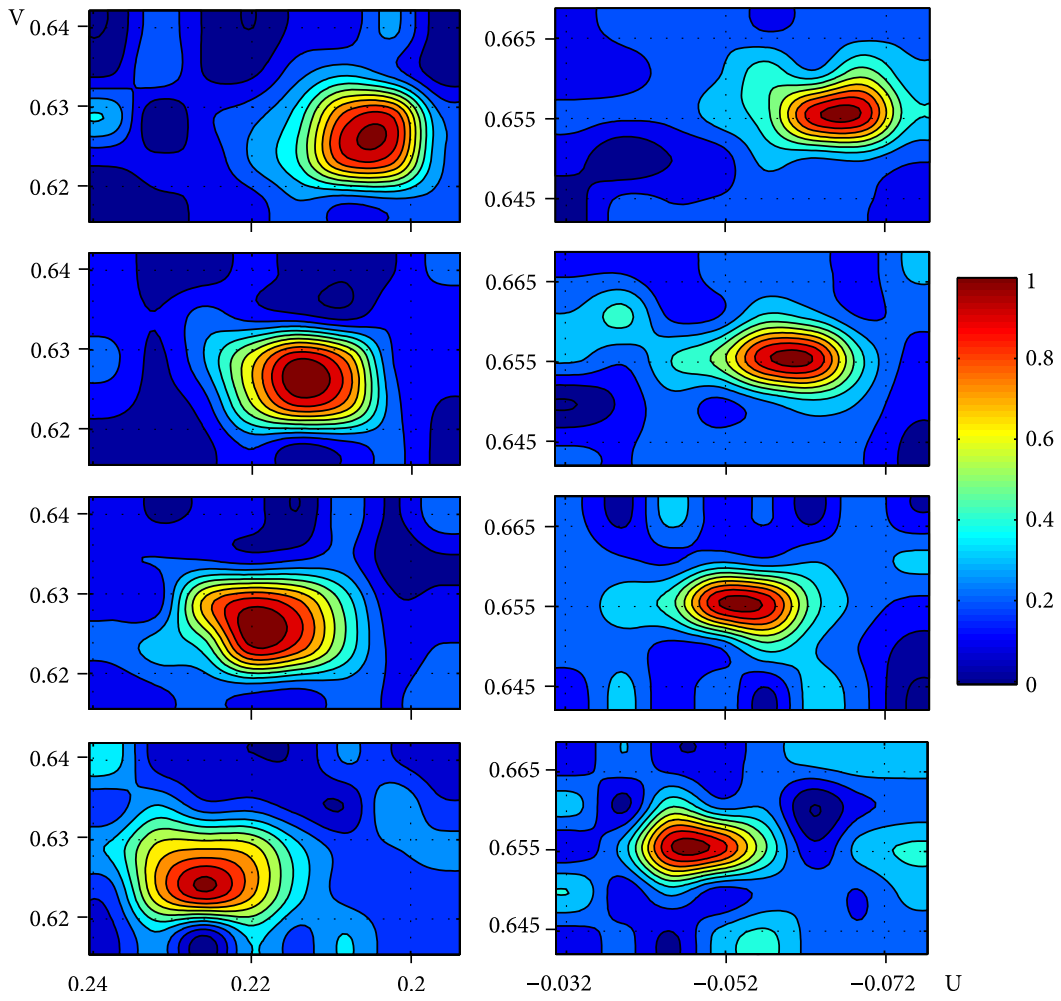

Fig. 2. Radio-frequency brightness distribution images of the solar corona. Left-side columns present measurement records obtained at 20 MHz about 10:00 UT on August 29, 2012; right-side columns present records obtained at 26 MHz about 09:12 UT on August 31, 2012. The four frames (top to bottom) demonstrate at each frequency the Sun's displacements in the sky resulting from daily motion of the celestial sphere. (Radiation intensity normalized to unity. Each of the frames obtained over 2 minutes of observations)

permitted us to observe the source passage from one beam of the frame to a neighboring beam in the next frame, thus showing the source to cross the entire frame. The UTR-2 antenna is directed so that the third (or central) beam captures the solar disk at the frame center. As a result, we could observe, due to the Earth's rotation, changes in the Sun position in every following frame in the sequence of heliograms. Although the UTR-2 heliograph has allowed recording solar radio images at 10—30 MHz, the frequencies were chosen so as to provide for the best interference immunity. Upon data reduction we obtained "dirty" images of the solar corona which represented a convolution of real solar corona images with the antenna pattern of the UTR-2. By utilizing a "clearing" procedure improved solar images could be obtained (Fig. 2). The calibration method was similar to such for the one-dimensional (1-D) heliograph observations. The contribution of refraction effects was small enough. The "clean" images gave us an opportunity to estimate angular sizes of the coronal diameters, both equatorial and polar, as well as integral flux densities and brightness temperatures. The coronal ellipticity ratio varied slightly during above period. The mean values of corona ellipticity were equal to about 0.75 and 0.73 at 20.0 MHz and 26.0 MHz, respectively. The diminishing brightness temperatures T_b of solar radio emission that were observed with a decrease of frequency can be explained by variations of the optical depth τ of the coronal plasma above the

emitting layer. In this case the electron temperature T_e of the corona (in the emitting layer) is almost constant ($\sim 10^6$ K for the given frequency range), while the distance from the Sun may increase. Then, according to the transfer equation, the relation $T_b = T_e(1 - e^{-\tau})$ shows a weak growth of the optical depth τ with increase in the frequency for the observations under consideration. Summarizing the 2-D heliograph observations, it can be argued that they seem to be in full agreement with the above represented results of 1-D heliograph observations. The structure of the solar corona is extremely dynamic in time and space. It is highly dependent on the solar activity level. During the period of minimum, the measured coronal density obeys the Newkirk model, while at times of high activity the Baumbach–Allen model is more suitable. In addition, the coefficients of these models are dependent on the positions of streamers, corona holes and active regions. Therefore, the problem of choosing a suitable model is relevant and greatly dependent on a specific research task. The elliptical model of the coronal electron density distribution has been investigated with the solar data analysis [13]. This model is most preferable for the study of the low-frequency emissions observable during solar activity minima. The results of observations that support the elliptical model of the coronal density (and are well known from the literature), allow us to estimate the characteristic parameters of such a model. Using the data of measurements, the electron density distribution can be described by the function $N_e = 10^{a+b/\rho}$ (where ρ is distance expressed in terms of solar radii), which is well known as the Newkirk model. In the equatorial plane, the model includes two independent regions, in which the function $N_e = 10^{a+b/\rho}$ has different coefficients as the distance ρ varies from 1 to 2 and from 2 to 6. The polar dependence of the electron concentration is described by the same function for $1 \le \rho \le 4$, however with different coefficients. The procedure for determining the parameters a and b from experimental data is very simple (namely, the least squares method). This gives a unique elliptic model of the solar corona, as regards the electron density distribution.

3. Type III Bursts

The type III solar bursts manifest themselves as radio emissions of a very broad frequency range, namely

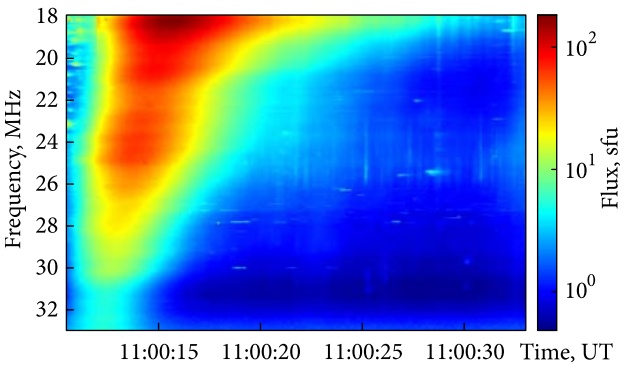

Fig. 3. Dynamic spectrum of the type III burst observed with the UTR-2 on June 2, 2011

from several gigahertz down to a few tens of kilohertz. They are generated by fast electron beams that propagate at velocities of about $0.3c$ (c is the velocity of light) along open magnetic field lines in the solar corona. The fast electrons induce Langmuir waves along the beam's propagation path, and the waves are scattered by ions and transformed into radio emission. The radiation mechanism is non-thermal, and therefore the radiation intensity increases with a decrease in frequency. Type III solar bursts are the largest population among the burst emissions. They have been observed since 1950s. The methods for observing the bursts practiced by the Institute of Radio Astronomy, NASU, have gone a long path of development from records at a few frequencies (namely, 10, 12.5, 16, 20, 24, and 30 MHz) to the use of 30-channel and 60-channel radiometers, and further on to broadband digital receivers (called DSP and ADR). The time and frequency resolutions of the latter have considerably improved quality of the data (Fig. 3). An important parameter of type III solar bursts is their frequency drift rate. It characterizes the velocity of burst sources (electron beams) in the solar corona. For many type III solar bursts within the range of 75 kHz to 550 MHz, the frequency drift rate takes the form $df/dt = -(0.01 \pm 0.008) f^{1.83\pm0.39}$. From observations of a group of type III radio bursts, a similar relation, specifically $df/dt = -0.0074 f^{1.76}$ is well known. Many other radio observations also have shown that the drift rate of type III bursts can be fitted to by a power-law function of frequency. As soon as the observations of July–August 2002, performed with the UTR-2 and a 60-channel radiometer, offered different results, this has aroused great interest. In this case the connection between the drift rate and fre-

quency for powerful type III bursts was allegedly linear, $df/dt = -Af + B$, with A and B varying from day to day. The contribution from B in df/dt could reach 33.3% at 10 MHz and 12.2% at 30 MHz. In this way, 163 bursts recorded in the July 2002 and 231 bursts of the August 2002 were analyzed. They covered the frequency range between 10 and 30 MHz. It should be noted that the multichannel analog spectrometer used in this experiment was tuned to 60 selected frequencies with a frequency bandwidth of 3 kHz in each frequency channel. However, the frequency channels had non-uniform spacing in frequency, and the frequency gaps between neighboring channels in the spectrometer varied from 110 kHz to 1.4 MHz, depending on the radio interference environment. Moreover, the 60 selected frequencies changed during the observations due to sporadically occurring radio interference, but these factors were not taken into account. All this raised doubts as to correctness of the results obtained. Moreover, the results of many years of observations (1973—1984) performed with the UTR-2 over the range of 12.5—25.0 MHz have shown the rate of the frequency drift to be proportional to power 1.7 of frequency and to slightly depend on the phase of the 11-year solar activity cycle (Abranin, Bazelyan, and Tsybko). Therefore, it seemed useful to check the frequency dependence of the drift rate in an alternative way [14]. For this purpose, we used the data obtained with one of the first digital receivers at our disposal. The digital receiver recorded the data in a 12 MHz continuous frequency band (from 18 to 30 MHz), with a 12 kHz frequency resolution and time resolution of 100 ms. In comparison with the 60-channel receiver, the number of frequency channels of the numerical receiver was much higher, reaching 1024. This allowed us to obtain significantly more data points for the analysis of frequency drift rates and other parameters of type III solar bursts.

During July—August 2002, the Sun made about two rotations. Many active regions (AR) were observed on the solar disk, from AR 10008 to AR 10096. The number of ARs varied from 4 to 13 in July, and from 7 to 14 in August. According to an overview of the strongest solar flares since June 1996, four events were recorded in July—August period of 2002. The greatest manifestation of solar activity was connected with ARs 10017, 10030, 10039, and 10069. They were likely responsible for the strong type III radio bursts observed at that time. The other ARs were not so burst-active. Using the digital receiver, we have analysed 214 bursts of July 2002 and 81 bursts of August 2002. When adjacent type III bursts overlapped so that they could not be distinguished from one another, such bursts were not taken into account in the analysis, because it was difficult to track their peaks separately. To estimate frequency drift rates of type III radio bursts of July—August 2002, we examined maxima of time profiles for the power spectral density for most of the bursts — if possible, between 18 and 30 MHz in each of the frequency channels. Normally, the frequency channels of the digital records that appeared clogged by narrow-band radio interference were ignored. The behaviour of the frequency drift rate is in direct connection with the mechanisms leading to emission of type III bursts. The type III bursts demonstrate a negative frequency drift rate because their sources (streams of fast electrons) originate from the Sun. They travel outward thorough the solar corona and produce radio waves at frequencies equal to the fundamental and second harmonic of the local plasma frequency, whereas the electron density of the solar plasma decreases with the distance from the Sun. We used the expression $f(t) = a(t - b)^{-\alpha}$ in the capacity of a fitting function. The parameters a, b, and α offered the best-fit result when the line could be drawn through the peak value of the flux for each type III burst on its dynamic spectrum and in each frequency channel. This representation has a clear astrophysical interpretation. If the radio emission source moves through the solar corona at a constant velocity v_b and at a negligible acceleration, it can travel a distance equal to $r(t) = r_0 + v_b(t - t_0)$, where r_0 is the initial position, and t_0 is the starting time. Generally, the beam velocity can vary along the entire propagation path of electron beams through the solar corona and the interplanetary space. Nevertheless, the assumption that any change in v_b was small at the heights where type III radio bursts were generated in the range of 10—30 MHz, is justified, and hence the change can be ignored. The background electron density $n_e(r)$ at the source location can be characterized by the local plasma frequency $f_p(r) = C(r/R_s - 1)^{-\alpha}$, where R_s is the solar radius. This source produces radio emission with a frequency drift in time, i.e., $f(t) = mf_p(r(t))$. According to the above equation, we have $a = mC(R_s/v_b)^{\alpha}$ and $b = t_0 + (R_s - r_0)/v_b$, with

$m = 1$ and $m = 2$ for the fundamental and higher order harmonics, respectively of the radio emissions belonging to a given burst. Next, the frequency drift rate for type III bursts is written as $df/dt = -Kf^{\nu}$, where $K = \alpha a^{-1/\alpha}$ and $\nu = 1+1/\alpha$. Based on the above procedure, we have found frequency drift rates of the type III solar bursts of July—August 2002. The fitting errors of K and ν of each individual burst were not taken into account, as they were too small. According to our data statistics, the values K and ν of the data set have skewed distributions. They are characterized by the mean value ($K = 0.0069$ and $\nu = 2.1$), mode ($K = 0.0051$ and $\nu = 1.85$), and median ($K = 0.0032$ and $\nu = 1.66$). Consequently, we have proven that the power-law dependence of the frequency drift rate upon frequency is typical of type III solar bursts. Commonly, the duration of type III bursts, described by the full width at half-maximum, increases toward lower frequencies (Wild, 1950). According to many solar radio observations from 300 kHz to 500 MHz, the duration is described by a power-law function of frequency. As applied to our data set, the dependence $\tau(f)$ is fit as $\tau = (6.07 \pm 2.26)/f^{0.743\pm0.42}$ (per 30 MHz). This result is once again in agreement with the results of other authors (for example, Reid and Kontar). According to the 60-channel observational data of the same period, the frequency dependence of type III burst durations was close to the reciprocal form $\tau = 200/f$. Thus, our analysis of frequency drift rates and durations of the solar type III bursts, recorded by the DSP in July—August 2002, has shown that the solar bursts have clear signatures typical of the well-known standard type III bursts. This is important because the dependence for the frequency drift rate as a power-law function of frequency is valid for weak, moderate and strong bursts. Regardless of the intensity of bursts, the electron beam's speed dependence on distance from the Sun is weak, and can be extrapolated from model representations. A possible explanation for the discrepancy between our conclusions and those obtained from the data of the 60-channel radiometer is that the latter contained notable omissions. Thereby, the simple linear model is underfitting to accurately capture the relationships between the frequency drift rates of solar type III radio bursts and their frequency, as well as the reciprocal form of their duration.

The pilot heliographic observations of solar bursts were fulfilled on April 9—11, 2013 for the frequency band 16.5—33.0 MHz [8]. At that time the solar activity was characterized by a large number of solar type III bursts. The low-frequency operating range enabled us to study upper layers of the solar corona. Therefore, we could observe characteristic spatial and temporal traits of coronal processes, particularly evolution of the angular structure of burst sources, at about 2—3 radii from the center of the Sun. At these heights angular dimensions of type III burst sources correspond to about one solar radius and even more. The operating rate of the output heliograph was one image per 3 seconds. The direction of the source motion through the upper corona was clearly detectable on the heliograms. Thus, the evolution was identified of the three-dimensional angular structure of type III solar burst sources (the time-dependent *UV*-plane frames at several selected frequencies).

4. Bursts with high-frequency cutoff

The type III bursts are the most numerous solar activity events manifesting themselves over the entire visible disk. However, the majority of observations are performed with the use of ground-based instruments, and a significant part of solar radio events remain unavailable for radio astronomy tools on the Earth. Space missions have allowed improving the situation, but the space-borne instruments are not as sensitive as the radio telescopes UTR-2, URAN, GURT and others. Nevertheless, radio emissions from some solar bursts on the far side of the Sun can arrive to ground-based telescopes due to special conditions in the solar corona. These are the bursts with a high-frequency cutoff (Fig. 4). Let us recall that the low-frequency cutoff effect (when frequencies below 10 MHz cannot reach ground-based instruments) for cosmic radio emissions appears due to the ionosphere. As for the high-frequency cutoff, its cause is totally different. That is explained by the burst's source position in the corona with respect to the observer. Indeed, if a source on the far side of the Sun is moved along the radial, it may be occulted by the solar corona. Therefore, the highest-frequency part of the solar burst spectrum is reflected away from the direction toward the Earth. The effects arising during propagation of the radio emission from behind-the-limb bursts in the corona affects time-frequency characteristics of such bursts as received during ground-based observations. Because type III bursts

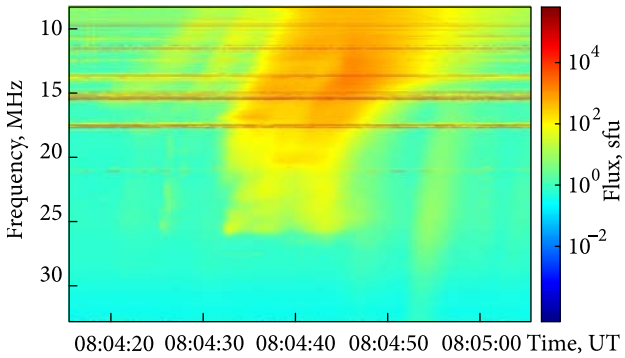

Fig. 4. Dynamic spectra of bursts with a high-frequency cutoff, recorded on August 18, 2012. The horizontal bright lines in the spectrum represent high intensity disturbances from broadcasting radios

are common, they are more likely to be detected with the high-frequency cutoff (under suitable conditions).

On August 19, 2012, starting at 8:23 UT, the UTR-2 recorded about a dozen of solar bursts that followed one another at 8 to 33 MHz [15]. Their main distinguishing feature was the high-frequency cutoff near the upper observation frequency for the UTR-2. We used only four sections of the "North-South" antenna array, and the radio data were recorded with the digital DSP spectrometer operating in the frequency range of 9—33 MHz. The time resolution was 100 ms and frequency resolution equaled 4 kHz. Some of these solar bursts had their cutoff frequency above frequency capabilities of UTR-2. To obtain a fuller view of all the events, we have examined the observational results from other two radio telescopes obtained at the same time, namely the French Nançay Decametric Array (10—70 MHz) and the Italian San Vito Solar Observatory of RSTN (25—180 MHz). Both instruments also showed the same bursts in their records. This allowed us to find cutoff frequencies for each burst. They were different from burst to burst in the range of 30—55 MHz. The frequency drift rate of the solar bursts was negative, 1.1—3.3 MHz s^{-1}, which corresponds to characteristic values for the decameter-wavelength type III bursts. The same is true for their duration. The flux densities shown by the events in the set never exceeded 1 000 sfu (1 sfu = 10^{-22} W m^{-2} Hz^{-1}), which suggests a moderate level of burst intensity. Thus, the solar bursts with a high-frequency cutoff can be identified as usual types III bursts that have been distorted by specific effects of radio wave propagation in the corona. Maybe, this is why the burst of June 3, 2011 looked like a "caterpillar".

Ray tracing for the solar bursts with cutoff, detectable in an inhomogeneous solar corona, requires special consideration. That was made in paper [16]. The propagation of radio waves through the solar corona, with account of electron density variations, can be studied in the framework of the geometrical optics approximation. Starting from simple assumptions, we have considered a spherically symmetric model of the electron density in the corona, using the approach described in the excellent paper by Bracewell and Preston (1956). By choosing a polar coordinate system with the origin coincident with the center of the Sun, one should be able to describe a ray trajectory in terms of two quantities, specifically the heliocentric distance ρ (expressed in solar radius units) and the angle θ between the directions toward a point on the ray trajectory and the observation point. Then Snell's law is represented in the form $n(\rho)\rho\sin\varphi = a$. Here $n(\rho)$ is the refractive index of the medium (coronal plasma), dependent on the magnitude of ρ, while the value φ represents the angle between the line tangent to the ray trajectory and the radius-vector to the point with the coordinates (ρ, φ). The distance between the ray's asymptote and its parallel line passing through the centre of the Sun is denoted as a. The refractive index $n(\rho)$ can be expressed in terms of the plasma frequency of the medium. Proceeding from simple geometric considerations, one can derive an expression for the trajectory in a differential form. As a result, the ray equation is obtained. The ray path has a turning point at an angle $\varphi = \pi/2$. In this case, the problem of calculating the ray trajectory and identifying the location of the turning point can be solved numerically. As for the electron density model for the coronal plasma, a variety of options exist. It is not difficult to find, from numerical simulations, that a ray may penetrate deep into the solar corona if being directed toward the center of the Sun. It is in this case alone that radio emission can reach the level in the corona (and be reflected there) where the plasma frequency of the surrounding medium is equal to the frequency of the probing radiation. If the incident ray arrives from a different direction, then it passes along trajectories in the corona that are noticeably higher than the height level corresponding to the plasma frequency. These features are pertinent to any

spherically symmetric coronal model with a monotonically decreasing electron density function. It turns out that the corona models we have considered all lead to restrictive conclusions regarding the possibility of observing behind-the-limb bursts. It must be taken into account that the radius of the Sun is 109 times the Earth's radius. A ray is directed toward the Earth, if the parameter a becomes very small. Accordingly, for the coronal models considered, detection of behind-limb bursts by ground-based instruments is hardly possible. Nevertheless, sometimes they happen to be observed, which means that in order to analyze the beyond-limb events, it is necessary to resort to other ideas about properties of the solar corona.

The next possibility that should be checked is to modify the spherical symmetry concept for the electron density in the corona. A more realistic model of the corona is an ellipsoid. To analyse the ellipsoidal model of the corona, one can use a piecewise linear approximation of a smooth ray trajectory, in which the corona is divided into layers, and the direction of refracted rays is derived from Snell's law. The main conclusion following from such an analysis is close to the previous conclusions. Ground-based instrumental detections of behind-the-limb bursts are, within this model of the corona, equally problematic. It should be noted that, based on the results of various observations, one can come to the conclusion that the structure of the real solar corona is strongly dependent on the state of solar activity, as well as on the processes occurring on the Sun and the corona itself (like solar flares, CME, etc.). Their effects on the number of electrons in the corona are quite significant. So, we have paid some attention to the contribution of CME on the effects of radio propagation in the solar corona, as applied to the behind-the-limb sources of bursts. What could be the reason for this? First, the observations of behind-limb bursts of August 17—19, 2012 were accompanied by numerous CMEs. Second, the CMEs themselves have very interesting properties, namely, they can generate cavities with a reduced electron density, which stay for a relatively long time. If such CMEs occur near the limb, then the cavities with a sufficiently low electron density may redirect the burst radiation from sources beyond the limb towards an observer on the Earth. Numerical simulations of ray tracing support this conclusion [16, 17].

This approach opens new research opportunities for estimating angular sizes of radio sources responsible for behind-the-limb solar bursts [18]. Usually, the sources of solar radio bursts are spatially resolved with interferometers and heliographs. The high-frequency cutoff effect of the solar bursts is caused by the occultation of their radiating sources for terrestrial observers. By studying the cases of radio occultation of low-frequency burst sources in the corona, we can arrive at an original method for filling-in gaps in our knowledge of low-frequency burst source sizes. The behind-limb burst records of August 17—19, 2012 have been used for the purpose. The high-frequency cutoff in solar bursts is somewhat similar to an occultation effect, with the difference that it originated owing to the solar corona rather than the Moon. In the general sense, the term "occultation" refers to either complete or partial obscuration of an astronomical object by another one. Also, let us recall that occultation effects regarding cosmic radio sources (for example, Taurus A, or the Crab Nebula) and the solar corona have been studied for many years. Just like the case of lunar occultations of radio sources, the limiting resolution is described by the width θ of the first Fresnel diffraction zone, $\theta = 0.5\lambda / D_M$, where λ denotes the observation wavelength and D_M is equal to the Earth-Moon separation length ($\approx 3.8 \times 10^8$ m). The radio occultation by the solar corona of low-frequency burst sources is characterized by a similar relation, namely $\theta = 0.5\lambda / D_S$, where D_S is the Earth-Sun distance ($\approx 1.5 \times 10^{11}$ m). Note that in the latter case the angular resolution of the interferometer is about 20 times higher than such for lunar occultations. The important advantage of this approach is that it enables determining the source size independently from the size of the radio antenna aperture used in the observation. From the study of radio profiles with a cut-off it seems very likely that diffraction effects are lacking. Thus, the difference between the frequencies f_1 at the starting point and f_2 at the end point (where the bursts may fall down in intensity, because of the cutoff, to the level of the background radio emission) is defined just by the angular size of corresponding sources at the given height level in the corona. If the values r_1 and r_2 for the frequencies f_1 and f_2, respectively, were known, then, using the relation $f\,[\mathrm{MHz}] \approx 9000\ \sqrt{N_e}\ [\mathrm{cm}^{-3}]$ and the electron density $N_e(r)$ of the solar corona in dependence upon the height r, the angular size of a

moving source may be estimated as $\theta_S \approx |r_1 - r_2| / D_S$. Unfortunately, the knowledge about the electron density of the solar corona has a semi-empirical character. There is a set of different models to describe the density fall-off with height, like those for the quiet equatorial corona, for active regions, or for coronal holes. The choice of the model affects both the resultant estimate for the height r and for the angular size θ_S derived. Therefore, we considered three popular models of coronal density (the so-called Newkirk, Baumbach-Allen and Mann), and compared their impact on the angular size. Another point of importance is that each burst with a high-frequency cut-off offers just one angular size of the source, corresponding only to its cut-off frequency. In our analysis, we find an "averaged" evolution of source sizes with frequency, using the cutoff frequencies of all the solar bursts observed at that time. Usually, the source size of solar bursts increases with decreasing frequency (as is well known, for example, for type III bursts). The evolution of the source size with frequency can be explained by broadening of electron beams due to the inhomogeneity of the solar corona. Following many observations at different frequencies, the source widths for type III bursts are fitted here by the power-law relation θ (arcmin) $\approx 659.4 / f^{0.97}$, where f denotes frequency in MHz. Note that the comprehensive study of type III radio source sizes at frequencies below 2 MHz that used the data of space-based observations (Steinberg et al., 1985), also gives a frequency dependence for the angular size of the source close to f^{-1}. Based on Newkirk's, Baumbach-Allen's and Mann's models of coronal density, average magnitudes have been established for angular sizes of behind-the-limb burst sources, specifically θ_N (arcmin) $\approx 157.8\, f^{-1.4}$, θ_{BA} (arcmin) $\approx 13.1 f^{-1.02}$ and θ_M (arcmin) $\approx 53.7 f^{-1.18}$, respectively. It should be pointed out that the Baumbach-Allen model is the best one those that suggest reciprocal power forms for the angular size dependences *versus* the observation frequency. However, there is a significant difference in the average source sizes of the behind-limb bursts and ordinary type III bursts. This can be explained by a less pronounced inhomogeneity of the solar corona for a given direction due to accompanying CMEs. Alternatively, this might result from solar burst focusing on low-density cavities in the CMEs. Estimating the average variation of solar burst size, for cases where the high-frequency cutoff was present, we have found the brightness temperature T_b of the radio source for the behind-limb burst at 08:05 UT. Over the frequency range considered, the highest brightness temperature of this burst reached about 7.1×10^{12} K which corresponds to brightness temperatures of type III solar bursts of moderate intensity. Note also that this burst is imposed on a background (thermal radio emission) with a brightness temperature of about 10^6 K.

The solar activity observed on August 17—19, 2012 was characterized by an emergence of a new group of solar spots near NOAA AR 11548 (N19E78 at 22:46 UT on August 18, 2012) on the far side of the Sun with respect to ground-based observations. This was due to the generation of many moderate flares over the eastern limb. August 19, 2012, was the final day for the series of repeated flares, when NOAA AR 11548 was on the near side of the Sun. A similar form of X-ray solar emission was noticed on August 17—18. Moreover, they were accompanied by repeated CMEs. To extend the data set of solar bursts with high-frequency cut-off, we used the observations performed with some other radio telescopes [19]. Despite the difference in characteristics of the radio astronomy instruments scattered around the world, all the radio records are of similar character, indicating that the high-frequency cutoff present in the bursts had is of solar origin rather than being due to the ionosphere and/or equipment malfunctions. In this case the spectral records represent a group of solar bursts morphologically similar to type III bursts. To see this more clearly, we have analyzed their frequency drift rate df/dt as a function of frequency. Having at our disposal 14 sets of hundreds of points, we sought for maxima of these bursts over time and frequency. For each set we have determined K and v for the above mentioned relation $df/dt = -Kf^v$. They correspond to standard values for ordinary solar type III bursts. According to our flux measurements, the solar bursts with high-frequency cut-off were moderate in intensity, as they only approached 1 000 sfu. Using the data set, burst's duration of staying at a frequency f can be written as $\tau = (120.3 \pm 55.8)/f^{0.56 \pm 0.21}$, consistent with the well-known results obtained for type III bursts. Thus, the simplest interpretation of solar bursts demonstrating a high-frequency cut-off is that their radiating sources move behind the solar limb relative to an observer on the Earth, while they are nothing else but type III bursts.

5. Type II Bursts

5.1. Fine structure

Type II solar radio bursts have been attracting the rapt attention of researchers (Fig. 5), because they occur during strong flares and are produced by shock waves that often escape into interplanetary space, reaching the Earth's orbit. They do not occur as often as type III bursts. In the decameter wavelength range (10—30 MHz), there was a gap in their studies until 2000 because of the absence of appropriate radio telescopes and of adequate recording equipment. As a result of an upgrade of the UTR-2 it became possible to fill this gap in. However, analysis of the fine structure of type II bursts has concerned so far only features like the herringbone structure and the irregular patchy structure in the shape of rapidly drifting spikes of short duration. Even these early results pointed to a great variety of features in the structure inherent in decameter type II bursts, and this problem required for separate attention in radio astronomical studies [20]. The fine structure of type II bursts in the form of drifting fibers that were observed in the frequency range of 17.5—29.5 MHz, with the aid of the 1024-channel digital spectrograph of the UTR-2, with a time resolution of 100 ms has been analyzed in detail for the first time. It should be noted that analysis of this fine structure suggests a clue to understanding the plasma processes in the corona. This is additional information on the propagation of shock waves escaping into the interplanetary space. Several type II radio bursts, at least two bursts in the meter-wavelength range and two interplanetary bursts (below14 MHz on the Wind/WAVES spacecraft), were observed after the small M2.4/SF flare at the western limb of the solar disk (active region AR 10061, N07W83) on August 16, 2002 (lasted from 05:46 until 06:37 UT). From the start of UTR-2 observations at 06:33:23 UT, the slowly drifting continuum was recorded at frequencies 12.5—19.0 MHz until 06:40:00 UT. The type II burst with a fine structure was observed with the UTR-2 after 07:20 UT in the frequency range 18.5—29.5 MHz. It was weak in intensity and had low frequencies, not detectable at frequencies above 30 MHz. Two CMEs were pointed out at that time. The first, slow CME propagated at a velocity of 493 km s^{-1}, starting from 05:30 UT. It preceded the shock wave responsible for the meter-wavelength type II burst at 05:52 UT. The second,

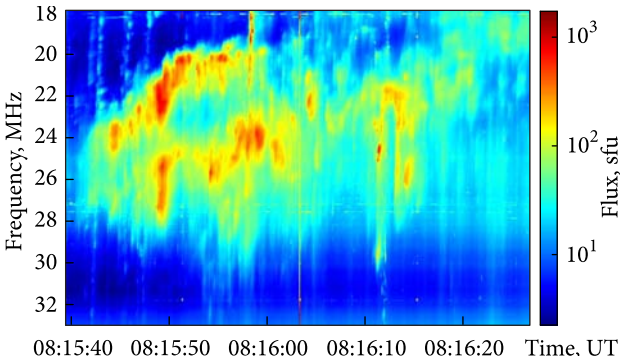

Fig. 5. Dynamic spectrum of the type II burst observed on June 2, 2011 with the UTR-2 radio telescope

faster CME of higher intensity was detected at 06:06 UT. It traveled at a velocity of 1 378 km s^{-1} and caught up with (and was absorbed by) the first CME at approximately 06:40 UT. The decameter-wavelength type II burst was in no way associated with the continuum burst that appeared at 06:30 UT in the Wind/WAVES observations and that continued in the form of patches until 07:30 UT. From LASCO C2 images a new narrow ejection was detected. By the time when the fine structure appeared, the leading edge of this new narrow CME had already gone far outside the range of altitudes corresponding to the UTR-2 frequency range (18—30 MHz). Thus, the fine-structured radio source observed in the UTR-2 spectrum could be in the tail of the narrow CME at the shock front. In the weak type II burst the fibers exhibit a most unusual fine structure, namely irregular broadband fibers (with a variety of instantaneous widths >250—500 kHz) with a superfine sub-structure in the form of narrow-band fibers (with band widths >50—90 kHz). The frequency separation of the latter rarely exceeds 50 kHz. Large fibers have a frequency drift rate $df/dt > -0.0365$ MHz s^{-1}, typical of type II bursts at these frequencies, while smaller fibers (within the large ones) have a frequency drift rates ranging from values almost equal to the drift rate of large fibers (parallel fibers at 07:22:30-50 UT in the largest fiber) to a minimum (on the average) value $>|-0.019|$ MHz s^{-1}. All larger-sized fibers have similar frequency drift rates, but they are spread randomly over the spectrum, with some of them exhibiting virtually no superfine structure. Narrow-band fibers are observed only in larger fibers. Five narrow parallel fibers produce a so-called rope of fibers, well known in the meter-wavelength range. It may

be distinguishable simultaneously in the largest fiber. In the event under consideration, the narrow fibers differ from the rope of fibers only by a slower frequency drift. The July 17, 2002 event was of considerable interest for comparison with the August 16, 2002 event described above, since it had a similar fine structure of radio emission (fibers), but was three orders of magnitude more intense. Meanwhile, the M8.5 flare occurred near the center of the disk (N21W17) in the huge active region AR 10030. The fragment of the type II burst at 17.5—29.5 MHz from the UTR-2 measurements contained two groups of fibers. The fiber frequency drift was approximately equal to that of the type II burst at 07:08:30 UT and was appreciably slower than that at 07:10:40 UT. This type II fiber burst occurred at the time when the shock caught up with the CME. This is in good agreement with the previous assumption about formation of a fine structure as the shock wave propagates in the CME tail. Following shock wave collision with the CME, the shock front velocity became almost equal to that of the CME (~650 km s^{-1}). Note that the fine structure in the form of fibers differs from such during the August 16, 2002 event by a shorter duration, ~20—30 s. The fibers in groups followed irregularly both in time and frequency. All of the fibers also differed in band widths, and appeared as individual bursts. The band width changed from its minimum value, > 0.028 MHz, to a maximum like 0.1 MHz. The frequency drift rate of the fibers in the first group was −0.08 MHz s^{-1}, i.e., lower than that of the patchy type II stripe with $df/dt > -0.11$ MHz s^{-1}. In the second group, the frequency drift rate was the same as shown by the large fibers on August 16, 2002, i.e. $df/dt > -0.036$ MHz s^{-1}. The fiber drift velocity of both events is assumed to be determined by the whistler group velocity inside the inhomogeneity in the CME tail.The whistlers excited at shock fronts manifest themselves only against the background of enhanced emissions from larger fibers, which might be the transition radiation from fast particles at inhomogeneities in the CME tail. The unusually low drift velocity of narrow fibers may be determined by whistler group velocity reduction in the inhomogeneity.

5.2. Absorption burst

On August 19, 2003 the UTR-2 radio telescope was used to observe (in absorption) a radio burst at 9—30 MHz against the background of solar type IV/II emission [21]. On that day the solar activity was moderate, representing just two M-class flares from AR 10431. At least six CMEs were registered. At 08:09 UT and 10:01 UT two type II bursts were observed. Next, during continuum radiation (type IV) one more type II burst occurred at 11:16—11:21 UT, with a sudden reduction in intensity. The absorption event lasted until 11:26 UT and demonstrated a clear negative frequency drift. The drift rate of the absorption burst was equal to -0.119 ± 0.008 MHz s^{-1} over the frequency range 14—30 MHz. That was four times greater than the drift rate of the corresponding type II burst, which was about −0.03 MHz s^{-1}. As can be seen, the absorption structure intersects with the underlying radio emission. Possibly, this implies that the absorber moved faster than the shock wave that generated the type II burst. In fact, the absorption feature seems to be superposed on the type IV continuum, which usually represents rising (CME-associated) structures. From 14 to 9 MHz the frequency drift rate of the absorption burst distinctly dropped to −(0.02—0.03) MHz s^{-1}. Against the background of the type II burst, fine structures were seen in the form of fibers (in emission), with a drift rate about −0.03 MHz s^{-1}. They disappeared and then appeared again in the absorption region on the background of the type II emission after the absorption had stopped. The duration of the absorption changed with frequency. Between 20 and 30 MHz it was approximately constant, showing a mean value nearly equal to 140 s, but from 20 to 14—15 MHz it dropped to ≈86 s, and then increased again. The measurement of duration was carried out with respect to a level that was twice as intense as the absorption burst minimum for each profile. The maxima of absorption on the time profiles correspond to a greater intensity reduction of the emission. How strong was it? On August 18, 2003 solar activity was at low levels. Therefore, we selected the pre-flare period of the August 19 observations as a representative record of the quiet Sun. Strictly speaking, the received emission contains not only the real emission from the quiet Sun but also the galactic background emission. The ratio between their intensities can be estimated. At the frequency of ≈25 MHz, the intensity of the absorption burst is close to 6.1×10^{-20} W Hz^{-1}, with that of the galactic background plus the quiescent-Sun level of 3.5×10^{-20} W Hz^{-1} and a proper galactic background level of 2.7×10^{-20} W Hz^{-1}. Then

the brightness temperature of the galactic background reaches ≈ 26 400 K. During the observation, the Sun was located in the sky region with a low temperature (brightness T) of the galactic background. According to our data, the galactic background's brightness temperature is expected to be around 27 200 K, which is in agreement with our estimates. It should be noted in this connection that the research facilities at the UTR-2 have had a sufficient dynamical range, and therefore any receiver saturation was unlikely. Alternatively, absorption processes in the ionosphere could be invoked to explain the appearance of the background-inflicted absorption of the radio emission from the Sun. Most of the attenuation occurs in the ionospheric D region (50 to 90 km above the Earth's surface), where the product of the electron density and the electron-neutral collision frequency reaches a maximum. Much more significant changes in the electron density, and consequently in the absorption strength, arise from solar X-ray flares (cf. the classic short-wave fade). However, no strong X-ray flares occurred, according to GOES data, between 11:00 UT until 12:00 UT on 19 August, 2003. Besides, we have found no manifestation of any extremely high absorption during the observation time at 9—30 MHz, judging by such ionospheric effects as sudden ionospheric disturbances and short-wave fadeouts. According to analyses of the event, the chain of processes responsible for the phenomenon could have developed as follows. Let us recall that the event started at 9:45 UT after the M-class flare. A piston shock wave propagated in the trace of the CME, and it was the source of the decameter-wavelength type II burst associated with absorption. In this case the electrons were accelerated by the type II shock and became trapped in slowly expanding loops behind the CME front. The shock wave traversed the loops at different heights. The absorption burst resulted in the development of a loss-cone instability in the system of "trapped and precipitating particles". The motion of the loops away from the Sun probably causes a negative frequency drift of the absorption burst.

5.3. Measurements of coronal magnetic-field strength

Plotting solar radio data in the form of a dynamic spectrum (intensity of radio emission *versus* both frequency and time) is a traditional approach to solar bursts visualization. Such pseudo-color 2D images permit one to distinguish one burst (or even a set of bursts) from other, as well as to determine their frequency drift rates and other parameters. Radio observations of solar activity at decameter wavelengths demonstrate a wide variety of solar bursts different in frequency, time, polarization and intensity properties. Consequently, analysis of solar burst records suggests the challenging task of understanding reasons why do such bursts appear together, how to separate the throng of different solar burst events into isolated bursts, and what kind of information about coronal properties could be found out. Therefore, a gradient analysis of the dynamic spectra has been applied to observational records of the complex structure of June 2, 2011 [22]. A dynamic spectrum of solar events, in the format of a pseudo-color image, consists of many structural units, such that an experimentalist often tries interpretation via simplified objects (tracks) or exaggerated features, in an attempt at facilitating clear perception and comprehension of the observed phenomena. Some of such basic units are pattern edges. These are recognizable through gradient differences on the images. Edges and their forms reflect a hierarchy of image structures, often looking like amazing ridges and valleys of a variety of scales. It turns out that the gradient processing is very useful for the study of crowded solar bursts via their images on dynamical spectra. The flexibility of gradient domain variation offers a high level of control in the gradient scale space, suppressing some of the scale features and amplifying other. The gradient domain is an intuitive representation for image contrast; where extremely steep edges (like Heaviside's step function) create remarkable discontinuities of the derivative associated with image brightness. Another source of gradient discontinuities is the noise present in all dynamic spectra. Solar bursts are always noise-like signals. Therefore, it is impossible to avoid smoothing of such an image. In this case, a very convenient approach is to form a convolution of the original spectrum with a Gaussian kernel. The Gaussian function is highly appropriate in the capacity of a smoothing kernel, because first, it is separable, and second its convolution with another Gaussian function leads to a Gaussian function again. Differentiating a convolution is a well-defined mathematical operation. It satisfies the important equality $(f * h)' = f * h' = f' * h$. Then the

gradient representation of the smoothing image can be calculated as a convolution of the original image with first order Gaussian derivatives, one for each dimension of the image, which can be determined explicitly. Consequently, we obtain two different scale spaces corresponding, respectively, to the horizontal and the vertical gradient. The extraction of different local orientation patterns is based on the calculation of gradients. The basic idea of reconstruction after a gradient-based processing is to find the unique solution of the corresponding Poisson equation. It is this idea that was used in the study of the June 2, 2011 event recorded by the UTR-2. The major feature of solar activity on that day was a series of solar X-ray flares following each other. The unusual set of bursts was observed from 06:55 UT to 07:05 UT in the frequency range 18.0–32.5 MHz. The dynamic spectrum consists of many horizontal strips imposed on vertical type III solar bursts. The maximum radio flux of the event reached ~100 sfu. In order to take away the vertical type III bursts from this dynamic spectrum, we used a gradient-domain filter. On the other hand, all the horizontal stripes might have been deleted by the same filter, just with another setting. This procedure gives us a chance for identifying the background which the horizontal strips hold on. The background radio emission has a negative frequency drift velocity, about ~0.062 MHz s^{-}. The value is typical for type II bursts at decameter wavelengths. Assuming that the background source was a shock wave, the mean shock speed can be estimated as 1 057 km s^{-1}. The background emission in the dynamic spectrum strongly correlates with the frequency-time position of horizontal strips, while showing no correlation with the vertical type III bursts. Thus, the shock wave can be related to a quasi-periodical structure. The zebra pattern (horizontal strips) and the band-split type II burst record of 08:15 UT both were analysed in an attempt of studying the coronal magnetic field within the height range of 1.9—2.0 solar radii [23]. Since we failed finding any harmonic structure for the type II burst present in the UTR-2 data, we assumed it was generated at the fundamental frequency. In addition, it allowed us to compare our results about the zebra pattern and the type II burst. The lower frequency branch (LFB) of the split band on the dynamical spectrum is caused by the emission coming from the region ahead of the shock (upstream region). That is characterized by an electron density n_1 and plasma frequency f_1, while the region behind the shock (downstream region) creates the upper frequency branch (UFB) of the split band. The latter region is compressed so that the electron density n_2 is higher than n_1 and the corresponding plasma frequency f_2 is higher than f_1. The instantaneous relative bandwidth (BDW) splitting is defined by the relation $\mathrm{BDW} = \Delta f/f = (f_2 - f_1)/f_1 = \sqrt{n_1 / n_2} - 1$. The density jump X across the shock is described by the value $(\mathrm{BDW}+1)^2$. According to the Rankine–Hugoniot jump relation, the Alfvénic Mach number can be expressed in terms of the density jump. From the frequency drift rate of the type II burst we find the shock speed, and then, profiting by the knowledge of the Mach number, it is easy to evaluate the Alfvén velocity and the ambient magnetic field strength B. The values obtained for the coronal magnetic field strength of 0.43 G seem to rather support the model of Gopalswamy than that of Dulk and McLean. These lower magnetic-field strengths may have resulted from a generally lower level of solar activity in Cycle 24. The next development of this approach concerned "fractured" type II radio bursts attributed to collisions of shock waves with the coronal structures giving rise to the solar wind [24]. The radio observations of two "fractured" type II bursts permitted us to estimate the magnetic field strength in solar wind structures. A detailed and careful analysis of the burst images and spectra has led to the conclusion that the radio source of the type II burst with a break point in its spectrum was placed at the shock nose, and the spectral shape observed resulted from the outward motion of the radio source through the pseudo streamer.

6.Type IV Bursts

6.1. Stationary type IV burst

The first of its kind radio image of a decameter-wavelength, stationary type IV solar radio burst has been obtained by processing the data of UTR-2 observations of Sept. 6, 2014 [9]. The event was investigated at that time with both space- and ground-based instruments. Spectral radio observations have been carried out with the radio astronomical facilities as follows:

• the ORFEES spectrograph of the Nançay Radio Observatory, France which operates in the range of 140-to-1 000 MHz;

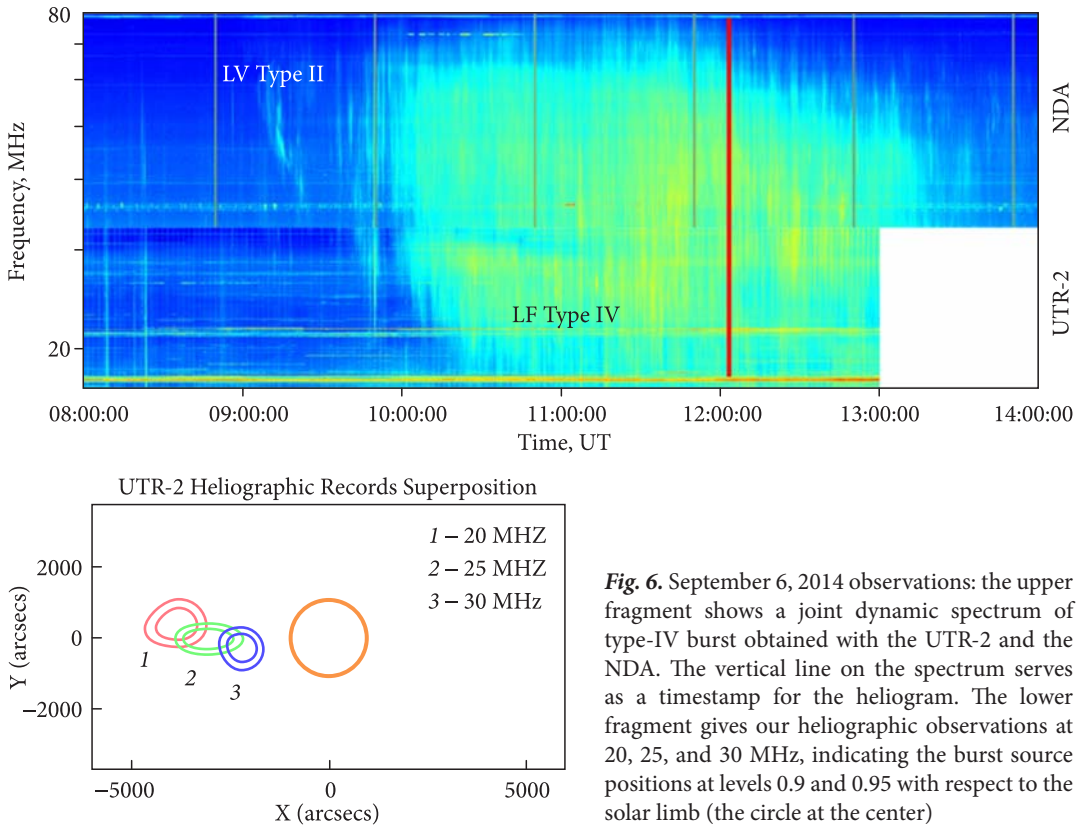

Fig. 6. September 6, 2014 observations: the upper fragment shows a joint dynamic spectrum of type-IV burst obtained with the UTR-2 and the NDA. The vertical line on the spectrum serves as a timestamp for the heliogram. The lower fragment gives our heliographic observations at 20, 25, and 30 MHz, indicating the burst source positions at levels 0.9 and 0.95 with respect to the solar limb (the circle at the center)

• the e-Callisto spectrograph, with three CALLISTO receivers fed by a bi-cone antenna (10—100 MHz) and a log-periodic antenna (100—200 MHz and 200—400 MHz) at the Rosse Solar-Terrestrial Observatory, Ireland (http://www.rosseobservatory.ie);

• the Nançay Decametric Array (France) utilized in the frequency range 10—70 MHz;

• the UTR-2 antenna array, Ukraine, designed for observations from 8 MHz up to 33 MHz.

The radio-frequency imaging was performed by the Nançay Radio Heliograph (NRF) at nine separate frequencies within the range of 150—445 MHz, and the UTR-2 heliograph at 16.5 to 33 MHz with a frequency resolution of 4 kHz [1—4]. Note that the results of highest interest results were obtained from low-frequency radio imaging measurements. On that day (Sept. 6, 2014) the CME onset was detected at 07:45:57 UT by the STEREO-Behind's EUVI camera. The observations showed that the CME started as a set of rising loops in the Active Region (AR) core. The eruption developed above the NOAA AR 12157 (S13 E57) containing 14 solar spots. The sunspot group had a complex magnetic structure (in $\beta\gamma\delta$ classification). The above mentioned CME onset coincides in time with the earlier growing phase of the successive class C8.0 X-ray flare from the said AR. Likely, the CME and the flare were connected with the same eruptive process on the Sun. At 10:12:00 UT and 10:54:26 UT the eruption was registered in coronagraph observations on both SOHO and STEREO spacecraft. According to the SOHO/LASCO C2, C3 and the STEREO COR2B measurements, the sky-plane (projected) speeds of the eruption were very close to each other in magnitude, namely about 414 km s^{-1} and 390 km s^{-1}, respectively. The CME is characterized by the angular width ~246 angular degrees, an almost constant linear velocity, and an acceleration about +0.5 km s^{-2}, according to the SOHO/LASCO C2, C3 observations. Moreover, the development of the eruption was accompanied both by coronal wave formation (most likely, a shock) and deflection of the coronal structure. Solar activity manifestations at radio frequencies were noticeable as a large number of high-frequency (HF) bursts, first appearing at ~ 08:40 UT and ending near 09:10 UT. The bursts are clearly visible in the ORFEES spectrum. Type II radio emission observable in the dynamic spectrum in the form of two

bursts, appeared after the type III bursts. We divided type II radio bursts into low-frequency (LF) and HF parts, where the latter showed a harmonic structure. The HF type II burst consisted of two branches (lanes), denoted as the fundamental (F) and the harmonic (H) components, with the H/F ratio about 1.9. The F and H bands started at ~09:12 UT as 224 MHz and 425 MHz emission lines, respectively. According to the dynamic spectrum, the fundamental radiation was restricted abruptly in frequency and time, at 144 MHz and at 09:22 UT, respectively, while the harmonic radiation lasted until 10:15 UT and has come to naught near 120 MHz. The frequency drift rate of the HF type II radio burst was about 0.122 MHz s^{-1}. The LF type II burst was represented in the NDA dynamic radio spectrum (Fig. 6). Following the records, the LF type II burst started just slightly before its HF companion. It originated at 09:01 UT near 67.2 MHz and continued until 09:23 UT at ~39.4 MHz. The frequency drift rate of the LF type II burst was about –0.024 MHz s^{-1}, which is typical of type II bursts at meter wavelengths.

The event of Sept. 6, 2014 was of interest not only because of the contribution from two type II bursts, but also because of the presence of continuum radiation over a wide frequency range. The continuum was separated quite apparently both on the HF and LF parts. Each of these demonstrates the special features representative of stationary type IVs radio emission. It is now believed that the origins, responsible for the long-lasting continuum in the solar radio emission, are the electrons moving in magnetic traps. As both the HF and LF type IVs bursts emerged from roughly the same area in the solar corona (see details below), it seems reasonable to assume their sources are to be the same. The LF type IVs radiation extended from meter to decameter wavelengths. In the decameter range the radio burst was observed with the 2D radio heliograph of the UTR-2 and some other antenna arrays.

The "North" and "South" arrays of the UTR-2 were also involved in the spectral measurements within 17—33 MHz, producing high-sensitivity solar dynamic spectra characterized by high resolution in time and frequency (~100 ms and ~4 kHz, respectively). The decameter radiation was observed for 3 hours, from 09:55 UT till the end of the observation session at 13:00 UT. The decameter continuum was similar to the steady irregular pattern seen in the dynamic spectra. Analysis of its fine structure revealed that the radio emission was composed of fragments like fiber bursts. The highest value of the radio flux density in the burst was about 100 sfu. At higher frequencies the radio emission was recorded with the NDA. Spectral records from the NDA showed a meter-wavelength stationary type IVs burst to have started at 09:50 UT. In about 5 minutes it became visible at decameter wavelengths as well. According to the UTR-2 spectral data, the stationary type IVs continuum radiation almost stopped, toward the end of observations, at low frequencies but lasted till ~13:20 UT at higher frequencies. Because of the strong radio frequency interference present in the NDA spectra below 30 MHz, spectral features of the stationary type IVs burst are not clearly recognizable. Meanwhile, the high sensitivity and high resolution of the UTR-2 allowed us to identify many spectral features of the bursts that are peculiar to this frequency range. Using the data, one can identify two enhancements of intensity (humps in the radio profiles) against the background of the decameter continuum. It should be pointed out that the emergence of two consecutive class C2.5 and class C1.7 solar flares from the NOAA AR 12157 coincided with these enhancements in time. To determine the start time for the HF type IV radiation, heliographic measurements turn out to be useful. The HF type IV source was observable since 09:48 UT at frequencies from 327 MHz to 173 MHz, and then at 150 MHz in the NRH records. The solar radio emission is seen as two bright regions. This can be explained as a manifestation of an earlier (prior to 09:48 UT) existence of a distinct radio source (the first of these regions). Next, the intensity of this emission decreased gradually, starting from the high frequency side, while another source, corresponding to the HF type IV emission, appeared almost immediately. This kind of development is observed in the consecutive NRH images as a jump in source locations. Consequently, the first moment of detecting the HF type IVs burst (at ~09:48 UT) was very close to the appearance in the spectral data of a LF type IVs burst (at ~09:50 UT). Furthermore, according to the NRH data after 13:10 UT there was a decline in brightness temperature profiles. The NRH maps show that the HF type IVs source disappeared completely towards ~13:40 UT at passbands from 327 MHz to 228 MHz, while at 150 MHz and at 173 MHz the brightness temperature decreased

by a factor of three in comparison with its value at 13:10 UT. This indicates that the LF type IVs burst emission presented in the NDA dynamic spectrum came to an end near 13:40 UT. Taking into account all the details of the above-stated evidence, we could assume the LF type IVs and HF type IVs bursts to have been events of the same origin.

6.2. Radio imaging

The UTR-2 radio heliograms were collected in a so-called three-dimensional (3D) cube built around two spatial coordinates and frequency. By making use of appropriate electron density models, one can determine heights of the corresponding emitting layers in the corona. While the total number of UTR-2 heliograms obtained between 09:55 UT to 13:00 UT in the observations at 16.5 to 33 MHz (4 096 spectral channels altogether, with a 3-sec frame cadence) is very high (about 1.5×10^6), there is no necessity to take the whole set of data into account. To observe changes of the source position in the solar corona, it is enough to take about fifty frequencies per each 3-sec frame. Next, we compared the UTR-2 heliograms with the corresponding NRH images. As far as the UTR-2 data are concerned, the uncertainty of measurements of the LF radio source is determined by the beam size of the antenna pattern. The imaging measurements show the locations of the radio sources to change as the CME propagates away from the Sun. The most obvious feature of this study is that the HF sources and the LF sources are in good alignment with each other above a CME-associated AR, apart from some kind of southward deflection of the LF parts taking place at certain instants. The LF type IVs radio emission was accompanied by a HF continuum. The presence of the latter is definitely confirmed by NRH maps and movies. The intensity variations, found in the decameter portion of the broadband type IVs continuum, are possibly affected by the number of energetic electrons, as well as the evolution of their velocity distribution function inside the radio emitting structure. It should be noted that there is another feasible scenario for the development of stationary type IV bursts, the one related to CMEs. In contrast to flares, which have relatively short characteristic times, a CME is a long-duration process. Such eruptions also involve processes capable of electron acceleration, which effect leads to type IV emission. For instance, in case an eruption is fast enough it can drive the shock ahead, or trigger magnetic reconnection along the post-CME current sheet, or else along certain magnetic separatrices within or about the eruptive structure. We assume this scenario to possibly play a role here. Very likely, the CME process may continue to induce acceleration of electrons, with further injection of the energetic particles into the type IV emitting structure (presumably a loop structure), in addition to those produced by the C8.0 flare. Note that the C8.0 flare, having a 1.5-hour-long declining phase, may continuously inject energetic electrons into the overlying magnetic structure. Then, it seems plausible that the HF and LF type IVs sources could emit from a single high-lying loop, at that with one foot located near the AR which the CME emerged from. The NRH measurements reveal motion of the HF emission source inside the magnetic loop which is close to its base. The UTR-2 heliographic images show very similar features, however at higher altitudes in the outer corona. According to the radio images obtained with the UTR-2, the uttermost altitudes of the layers emitting at 20 MHz, 25 MHz, and 30 MHz were around $4.5R_S$, $3.9R_S$, and $3.0R_S$, respectively. The declined southward deflection and the ascent-and-descent motion may represent the response of the presumed loop structure to CME-provoked disturbances, including dynamical displacements of the structure and the changing inner density or appearance of turbulent levels.

Conclusions

In this paper, we have presented a detailed study of solar radio emissions at decameter and meter wavelengths, using the data obtained from long-term observations with Ukrainian radio telescopes. These results are most interesting and fundamental. The sphere of investigations includes both thermal and sporadic components observable during the 11-years solar cycle in different phenomena of the solar activity. The observational solar radio astronomy, like radio astronomy in general, is based on passive experimentation, in the sense that we cannot change anything in astrophysical processes or their responsible conditions, while only being able to carry out observations, either remote or, occasionally, in-situ. It often takes a long time (in human terms), but the

data processing takes even longer. Another obstacle is that the UTR-2 observations are commonly performed during summer months and from 07:00 UT to 14:00 UT. This is due to the fact that at these time periods the solar observations can be done to the best sensitivity of the telescope, as the radio antenna manifests its most effective characteristics. Recently, the URAN-2 array was used for monitoring the Sun throughout the year. As a result, we have obtained a huge amount of records in many high-capacity hard drives. Their processing takes time, and the volume of data is constantly growing. The transition from manual work with the data to faster, automated collection and processing is highly relevant. On the agenda are pattern recognition, complex statistical processing, cluster analysis, neural networks, and machine learning. Although they are not an end in themselves, their implementation and verification in different cases can revolutionize the study of solar radio emission.

Solar radio studies have been going on for many decades. Technological leaps lead to re-estimation of the goals and objectives of such research. What seemed impossible before has now been commonplace. Every now and then it is useful to realize new challenges to the experimental study of low-frequency solar radio emissions. Let us give our investigations their present essence. Daytime observations concern not the Sun alone, but also other cosmic radio sources (Jupiter, pulsars, 3C461, etc.). In this situation, we have to choose what to observe. Quite often we cannot know in advance, exactly which type of solar bursts is to be expected. Purposeful observations of solar bursts could allow us understanding whether and how their properties do or do not change during the solar cycle. The evolution experienced by the solar corona because of activity processes (which are its most variable feature), affects directly the time and frequency properties of the solar bursts generated there. It was noticed that many CMEs prevent generation of such bursts. Moreover, they require a special configuration of magnetic fields in the active regions. All this determines the conditions under which solar radio emissions get "prepared for presentation". Another example occurs, when the Sun is quiet. Single type III bursts are very popular at that time. In any case the prediction of observable types of solar bursts would be desirable. Currently, the approach to this problem is still empirical, but when we do understand better the mechanisms responsible for one or another type of bursts, the puzzle will be resolved. Additionally, it would be better to have observations of solar bursts with a high enough temporal resolution, but they take up a lot of space on electronic memory devices. With regard to the features of the UTR-2 heliograph, its design could be transferred into the parallel mode so as to permit it operating independently of the usual spectral mode. That would allow switching the heliograph on and off in dependence of solar activity during a day of observations, thus making our observations more effective.

The UTR-2 cannot support polarization measurements, whereas the URAN-2 and the GURT can. Such measurements are among the most difficult in low-frequency radio astronomy, as they require careful calibration and debugging. Our knowledge of polarization properties of the solar bursts would make it possible to understand the mechanisms leading to generation of the variety of the types observed. On the other hand, solar bursts serve as probing signals for investigating the solar corona. A thorough analysis of solar bursts could provide information not only on their generation mechanisms, but on the medium (corona) through which the radio emission propagates. Currently, this is a task of unimaginable complexity because of insufficient knowledge about the corona properties and the mechanisms of solar burst generation.

This work was supported within the Space Research Program of the National Academy of Sciences of Ukraine (State registration numbers 0122U002459 and 0122U002460).

The authors are grateful to Prof. N.G. Shchukina for her useful comments.

REFERENCES

1. Stanislavsky, A.A., Abranin, E.P., Konovalenko, A.A., and Koval, A.A., 2011. Heliograph of the UTR-2 radiotelescope. Part I: General scheme. *Radio Phys. Radio Astron.,* **2**(3), pp. 197—204. DOI: 10.1615/RadioPhysicsRadio Astronomy.v2.i3.10
2. Abranin, E.P., Stanislavsky, A.A., Koval, A.A., and Konovalenko, A.A., 2011. Heliograph of the UTR-2 radiotelescope. Part II: Design features. *Radio Phys. Radio Astron.,* **2**(4), pp. 299—305. DOI: 10.1615/RadioPhysicsRadioAstronomy. v2.i4.20
3. Koval, A.A., Konovalenko, A.A., and Stanislavsky, A.A., 2011. A new heliograph of the UTR-2 radio telescope: design and performance. In: *2011 XXXth URSI General Assembly and Scientific Symposium Proceedings.* Istanbul, Turkey, 13–20 Aug. 2011. DOI: 10.1109/URSIGASS.2011.6051199
4. Konovalenko, A.A., Stanislavsky, A.A., Koval, A.A., and Abranin, E.P., 2012. Heliographofthe UTR-2 radiotelescope. III. Observations. *Radio Phys. Radio Astron.*, **3**(1), pp. 1—5. DOI: 10.1615/RadioPhysicsRadioAstronomy.v3.i1.10
5. Stanislavsky, A.A., Koval, A.A., Konovalenko, A.A., and Abranin, E.P., 2011. *Heliograph of the UTR-2 radiotelescope*. https: //arxiv.org/abs/1112.1044.
6. Stanislavsky, A.A., Konovalenko, A.A., Koval, A.A., and Volvach, Ya.S., 2018. An upgrade of the UTR-2 radio telescope to a multifrequency radio heliograph. *Sun Geosph.*, **13**(1), pp. 21—24. DOI: 10.31401/SunGeo.2018.01.03
7. Stanislavsky, A.A., Koval, A.A., and Konovalenko, A.A., 2013. Low-frequency heliographic observations of the quiet Sun corona. *Astronom. Nachr.*, **334**(10), pp. 1086—1092. DOI: 10.1002/asna.201211839
8. Koval, A.A., Stanislavsky, A.A., Konovalenko, A.A., and Volvach, Ya.S., 2014. Tracking Type III radio burst sources in the solar corona by heliographic means. *Odessa Astron. Publ.*, **27**(1), pp. 74—75. DOI: 10.18524/1810-4215.2014.27.81247
9. Koval, A.A., Stanislavsky, A.A., Chen, Y., Feng, Sh., Konovalenko, A.A., and Volvach, Ya.S., 2016. A decameter stationary type IV burst in imaging observations on the 6th of September 2014. *Astrophys. J.*, **826**(2), id. 125. DOI: 10.3847/0004-637X/826/2/125
10. Koval, A.A., 2011. Analysis of quiet-Sun radio observations using the decametric telescope UTR-2. *Astronomical School's Report*, **7**(1), pp. 34—41 (in Russian). DOI: 10.18372/2411-6602.07.1034
11. Brazhenko, A.I., Koval, A.A., Konovalenko, A.A., Stanislavsky, A.A., Abranin, E.P., Dorovskyy, V.V., Melnik, V.M., Vashchishin, R.V., Frantsuzenko, A.V., and Borysyuk, O.V., 2012. Peculiarity of continuum emission from upper corona of the Sun at decameter wavelengths. *Radio Phys. Radio Astron*., **3**(3), pp. 187—196. DOI: 10.1615/RadioPhysicsRadioAstronomy.v3.i3.10
12. Konovalenko, O.O., Koshovyy, V.V., Lozynskyy, A.B., Stanislavsky, A.A., Shepelev, V.A., Ivantyshyn, O.L., Kharchenko, B.S., Lozynskyy, R.A., Brazhenko, A.I., Abranin, E.P., and Koval, A.A., 2012. Quiet Sun observations by the URAN-2 and URAN-3 decameter radio telescopes during the solar eclipse of August 1, 2008. *Radio Phys. Radio Astron*., **17**(4), pp. 295—300 (in Ukrainian).
13. Stanislavsky, A.A., and Koval, A.A., 2013. Solar corona elliptical model. *Radio Phys. Radio Astron*., **18**(1), pp. 3—11 (in Ukrainian).
14. Stanislavsky, A.A., Konovalenko, A.A., Abranin, E.P., Dorovskyy, V.V., Lecacheux, A., Rücker, H.O., and Zarka, P., 2018. Revisiting the frequency drift rates of decameter type III solar bursts observed in July — August 2002. *Sol. Phys.*, **293**(11), id. 152. DOI: 10.1007/s11207-018-1374-6
15. Stanislavsky, A.A., Konovalenko, A.A., Volvach, Ya.S., and Koval, A.A., 2015, High-frequency cut-off in type III bursts. *Odessa Astron. Publ.*, **28**(2), pp. 246—247. DOI: 10.18524/1810-4215.2015.28.71043
16. Stanislavsky, A.A., 2016. The role of radio wave propagation effects in the solar corona to interpret the behind-limb bursts. *Radio Phys. Radio Astron.*, **21**(1), pp. 3—13. DOI: 10.15407/rpra21.01.003
17. Stanislavsky, A., Konovalenko, A., Koval, A., Volvach, Y., and Zarka, P., 2016. CMEs and frequency cut-off of solar bursts. *Sun Geosph.,* **11**(2), pp. 91—95.
18. Stanislavsky, A.A., Konovalenko, A.A., Volvach, Ya.S., and Koval, A.A., 2017. Brightness temperatures of solar bursts with high-frequency cut-off. In: G. Fischer, G. Mann, M. Panchenko, and P. Zarka, eds. *Planetary Radio Emissions VIII*. Proc. 8th Int. Workshop on Planetary, Solar and Heliospheric Radio Emissions held at Seggauberg near Graz, Austria, 25—27 Oct. 2016. Vienna: Austrian Academy of Sciences Press, pp. 391—401. DOI: 10.1553/PRE8s391
19. Stanislavsky, A.A., 2017. Solar type III bursts with high-frequency cut-off. *Astron. Nachr.*, **338**(4), pp. 407—412. DOI: 10.1002/asna.201613141
20. Chernov, G.P., Stanislavsky, A.A., Konovalenko, A.A., Abranin, E.P., Dorovsky, V.V., and Rücker, H.O., 2007. Fine structure of decametric type II radio bursts. *Astron. Lett.*, **33**(3), pp. 192—202. DOI: 10.1134/S1063773707030061
21. Konovalenko, A.A., Stanislavsky, A.A., Abranin, E.P., Dorovsky, V.V., Mel'nik, V.N., Kaiser, M.L., Lecacheux, A., and Rücker, H.O., 2007. Absorption in Burst Emission. *Solar Phys*., **245**(2), pp. 345—354. DOI: 10.1007/s11207-007-9049-8
22. Stanislavsky, A.A., Konovalenko, A.A., Koval, A.A., Dorovsky, V.V., Zarka, P., and Rücker, H.O., 2015. What can be interesting in the analysis of crowded solar bursts? *Sun Geosph.*, **10**(1), pp. 17—20.
23. Stanislavsky, A.A., Konovalenko, A.A., Koval, A.A., Dorovskyy, V.V., Zarka, P., and Rücker, H.O., 2015. Coronal magnetic field strength from decameter zebra-pattern observations: Complementarity with band-splitting measurements of an associated type II burst. *Sol. Phys.*, **290**(1), pp. 205—218. DOI: 10.1007/s11207-014-0620-9
24. Koval, A., Karlicky, M., Stanislavsky, A., Wang, B., Barta, M., Gorgutsa, R., 2021.Shock-wave radio probing of solar wind sources in coronal magnetic fields. *Astrophys. J.*, **923**(2), id. 255 (10 pp.). DOI: 10.3847/1538-4357/ac2f3f

Received 02.06.2022

О.О. Станиславський[1], А.О. Коваль[2], І.М. Бубнов[1], А.І. Браженко[3]

[1] Радіоастрономічний інститут НАН України
вул. Мистецтв, 4, м. Харків, 61002, Україна
[2] Astronomical Institute of the Czech Academy of Sciences
Fričova 298, 251 65 Ondřejov, Czech Republic
[3] Полтавська гравіметрична обсерваторія Інституту геофізики
ім. С.І. Субботіна НАН України
вул. Мясоєдова, 27/29, м. Полтава, 36029, Україна

ДОСЯГНЕННЯ У ВИВЧЕННІ ДЕКАМЕТРОВОГО РАДІОВИПРОМІНЮВАННЯ СОНЦЯ ЗА ДОПОМОГОЮ УКРАЇНСЬКИХ РАДІОТЕЛЕСКОПІВ. Частина 1

Предмет і мета роботи. Наведено результати досліджень сонячної корони з використанням всесвітньо відомих українських радіотелескопів. Метою роботи є послідовний огляд нещодавніх досягнень у спостереженнях різних типів низькочастотного радіовипромінювання Сонця.

Методи і методологія. Дослідження спокійного (теплового) і спорадичного (спалахового) радіовипромінювання Сонця проведено на радіотелескопах декаметрового діапазону УТР-2, ГУРТ і УРАН-2. Викладено особливості низькочастотного сонячного радіовипромінювання від різноманітних джерел, з характеристикою оптимізованих методик, які були застосовані в кожному випадку для оцінки фізичних параметрів корони в зонах генерації радіохвиль декаметрового діапазону.

Результати. Аналіз часових, частотних і просторових характеристик сонячного радіовипромінювання дозволив запропонувати низку моделей розподілу електронної щільності в короні та оцінити напруженість магнітного поля в короні. Отримані нами експериментальні результати узгоджуються з даними спостережень, що були виконані в різних частотних діапазонах і з використанням як наземних, так і космічних приладів.

Висновки. Радіочастотні спостереження на українських радіотелескопах дозволяють досліджувати радіовипромінювання Сонця від різних локальних джерел з високою часовою, частотною та просторовою роздільною здатністю. Разом з великою ефективною площею та чутливістю антен це дає змогу застосовувати широке коло методів і засобів для аналізу сонячних сплесків різної інтенсивності на фоні земних завад природного та штучного походження.

Ключові слова: *Сонце, декаметрове радіовипромінювання, радіосплески, сонячна корона, УТР-2, УРАН-2, ГУРТ.*